ISSN: 2160-049X Volume 7, Number 9, September 2017

Scientific Research Publishing

World Journal of Mechanics

ISSN: 2160-049X
9 772160 049007 09

www.scirp.org/journal/wjm

Journal Editorial Board

ISSN 2160-049X (Print) ISSN 2160-0503 (Online)

http://www.scirp.org/journal/wjm

Editors-in-Chief

Scientific Research Publishing

World Journal of Mechanics, 2017, 7, 243-270
http://www.scirp.org/journal/wjm
ISSN Online: 2160-0503
ISSN Print: 2160-049X

Table of Contents

Volume 7 Number 9 September 2017

World Journal of Mechanics (WJM)
Journal Information

SUBSCRIPTIONS

The *World Journal of Mechanics* (Online at Scientific Research Publishing, www.SciRP.org) is published monthly by Scientific Research Publishing, Inc., USA.

Subscription rates:
Print: $69 per issue.
To subscribe, please contact Journals Subscriptions Department, E-mail: sub@scirp.org

SERVICES

Advertisements
Advertisement Sales Department, E-mail: service@scirp.org

Reprints (minimum quantity 100 copies)
Reprints Co-ordinator, Scientific Research Publishing, Inc., USA.
E-mail: sub@scirp.org

COPYRIGHT

PRODUCTION INFORMATION

For manuscripts that have been accepted for publication, please contact:
E-mail: wjm@scirp.org

Scientific Research Publishing

World Journal of Mechanics, 2017, 7, 243-254
http://www.scirp.org/journal/wjm
ISSN Online: 2160-0503
ISSN Print: 2160-049X

Studying of Kinematics and Elements of Tension of Blocks of the Massif According to Field Geological Observations

R. A. Umurzakov[1], M. Yu. Muminov[2]

[1]Tashkent State Technical University, Tashkent, Uzbekistan
[2]Institute of Seismology of Academy Sciences of Republic Uzbekistan, Tashkent, Uzbekistan
Email: umrah@mail.ru, tashkent@seismo.org.uz

How to cite this paper: Umurzakov, R.A. and Muminov, M.Y. (2017) Studying of Kinematics and Elements of Tension of Blocks of the Massif According to Field Geological Observations. *World Journal of Mechanics*, **7**, 243-254.
https://doi.org/10.4236/wjm.2017.79020

Received: August 9, 2017
Accepted: September 16, 2017
Published: September 19, 2017

Abstract

The description of the received new results of field geological (tectonophysical) study of massifs of rocks is provided: tectonic jointing, explosive and folded deformations, mirrors of slidings, tectonic motions of blocks of breeds. Reconstruction of fields of tension according to geological data of the certain massif of the Chatkalo-Kurama mountain area (Tien-Shan)—a coastal zone of the Charvak reservoir and the Almalyk mining industrial region is executed. The multidirectional motions of blocks of rocks in the massif of a coastal zone of the Charvak reservoir connected with tectonic and technogenic factors are revealed. The scheme of kinematics and the intense deformed condition of blocks of the Almalyk district is received. Here the regional field of tension with horizontal and submeridional orientation of an axis of the main normal tension of compression at the inclined provision of two other axes are observed. The received results testify to opportunities field the tectonophysical of methods for obtaining important data on kinematics and dynamics of massifs of rocks, tectonic blocks, and features of their deformation. Such studying of the massif of rocks before the beginning and in the course of performance of work on objects of the national economy is important for the choice of design and optimum parameters of laying of excavations, control of a condition of their boards and walls, definition of strategy of safety of conducting mining operations and also seismic stability of constructions.

Keywords

Massif of Rocks, Structure, Kinematics, Dynamics, Tectonophysics, Deformations, Mirrors of Slidings, Field of Tension

1. Introduction

In massifs of rocks under the influence of a force field there are motions of blocks which in mining literature call "displacement" of blocks. These shifts leave a mark in exposures of breeds on the planes of shifts in the form of various furrows, lines, strokes, forming small and large surfaces—mirrors of slidings (slickensides). They have quite wide circulation and are used by geologists when studying character of shifts on the separate planes of explosive violations, cracks, etc. Such data on mirrors of slidings have been used by certain researchers (J. Angelier, France) for reconstruction of stress of sites of crust [1] [2] and also the Russian researchers [3] [4]. Such approach has been used also by authors of article for reconstruction of fields of tension of crust of certain areas of the Western Tien Shan. However, in difference from the previous researchers on the basis of use of these mirrors of sliding the method of kinematic reconstruction of late Cainozoic shifts of tectonic blocks has been developed (R. Umurzakov). This method has been used for studying of a tectodynamics of certain regions of Tien Shan, also the epicentral of areas of strong earthquakes [5] and also massifs of boards of large reservoirs, areas of development of mineral deposits. The analysis of the published literature shows that on sites of developments of mineral deposits the geodynamic approach based on the analysis of data of a relief [6] is used so far. Such approach can't give a real picture of geodynamics and stress of the massif on sites of the developed fields. For ensuring stability of boards of pits, more fundamental approach with identification and accounting of tectonic factors is necessary for safety of conducting mountain developments. The importance of these researches for mining is defined as well by use of knowledge of tension in the search purposes. For example, for forecasting of location of the hidden ore bodies, definition of spatial orientation of the weakened zones and orientation of hydrodynamic processes, a fluid current. These data matter also at researches of parametrical factors of stability of tunnels [7], for forecasting of formation of a karst [8], research of zones of breaks [9], etc.

All this defines relevance and the practical importance not only separate local definitions, but also identification of regional features of the field of tension that is a subject of the special scientific direction in geotectonics and geodynamics—"tectonodynamics" [10] [11].

The description of the received new results of field study of tectonic jointing, other types of deformations, tectonic motions of blocks of rocks, reconstruction of fields of tension according to field geological data on the example of the certain massif of an orogen of Tien Shan (Chatkal-Kurama mountain area) is provided in this article.

2. Methodology and the Used Material

When studying kinematics of blocks of rocks data on shifts on mirrors of slidings (slickensides) were used. Receptions of the description and identification of useful information on mirrors of sliding are in details described in educational

geological literature. About opportunities of use of these mirrors of sliding on local points of observations for reconstruction of tension are described in works [1] [2] [3] [4] [5]. For reconstruction of kinematic motions of blocks the "technique of kinematic reconstruction of shifts of blocks" [12] developed by the author of the present article is used. It consists in definition of the general component of a motion for all studied block according to local data of separate points of observations. The technique allows studying features of kinematics of tectonic blocks of massifs of rocks of the bases of reservoirs, boards of pits and vicinities of excavations and also for the purpose of study of elements of geodynamics and a seism geodynamics of certain areas. Possibilities of use of a technique when determining the mechanism of the centers of earthquakes were discussed by us in work [5].

As the main material for definition of kinematics of blocks serve measurements of parameters of shifts (slickensides) in local points. In each point of observation the quantity is from 6 - 12 before measurements. Local points are grouped in tectonic blocks which are defined on the basis of geological inspection of the site. Features of section of massifs of rocks are studied by larger explosive violations, zones of breaks. On the basis of local these points the total component of the direction of a motion of the block is defined. For this block definition of axes of the main normal tension is carried out.

3. Results and Discussion

3.1. Studying of Kinematics and Dynamics of Blocks near a Reservoir

When study behavior of the massif of rocks of the basis of a dam in a coastal part of the Charvak reservoir (Uzbekistan, the Tashkent region) it has been established that separate blocks test multidirectional shifts. It is necessary to tell that study of deformation processes of boards of reservoirs has special relevance. It is connected, first of all, with the solution of tasks of ensuring geoecological safety. The Charvak reservoir is the largest in Uzbekistan. Water volume at the maximum filling can reach about 2 billion cubic meters. The bowl of a reservoir is dated for the Burchmulla hollow delineated by slopes of Ugam, Pskem, Koksu and Chatkal ridges. The river Chirchiq originates from the dam. On the site near a reservoir the valley is crossed by three largest zones of explosive violations of northwest pro-deleting which have distinct expression in a relief. On all three zones the left moving is characteristic that is visible also on signs in a relief. Noted zones of breaks form a step relief with different hypsometric situation the terrace of surfaces (Q_2) that testifies to comparative youth of movements.

The fact that the right board of a reservoir, and in a middle part, and at a dam, is put by powerful thickness of cenozoic deposits attracts attention. They are presented in the lower part of a section sandstone-gravelite and a lime-sandstone pack the paleogene-neogene of deposits on which the loess and loamy deposits, conglomerates and pebble of quaternary age lie. The left (southern) board of a

reservoir with traces of some complications is composed by Paleozoic educations which in places are blocked by MZ-KZ-deposits. All bowl of a reservoir, being in a zone of the largest breaks of N-W of orientation named by Kumbel-Ugam it is cut by explosive violations of different orders. Presence of shift shifts on the Kumbel-Ugam zone of breaks has led to narrowing of the valley Chatkal in the form of a canyon where actually and the dam alignment is dated. Detailed studying of a structural and dynamic situation of a coastal zone of a reservoir on the basis of a complex of structural and geological observations with attraction of methods of a field tectonophysics has allowed revealing the following.

It is revealed and studied several ranks of disjunctive violations: jointing of rocks and their kinematic parameters; large cracks, secants exposure, and shifts on them; large linearly—the extended zones of crushing of the massif of rocks with elements of shift shifts in the basis of a dam, left (southern) and right (northern) reservoirs of coastal boards.

The basis of a dam is put by strongly shattered breeds of middle paleozoic age (the lower carbon fabrics, mainly limestone). Directly at a dam alignment, in the item of point of observation (p.o.) 1 (**Figure 1**), they lie down with the dip azimuth 0˚ angle 60˚. To the South they gradually change falling on dip Az 15˚ angle 65˚ and further, in the item of p.o. 2 on dip Az 20˚ angle 55˚. In places they strongly shattered and weathered and bedding elements don't manage to be determined by primary observations. Exposure cuts a set of cracks of the different sizes and spatial orientation.

In a northern board of a reservoir near a dam, the multidirectional planes of cracks of northeast and northwest strike, with the prevailing falling of their planes to the southwest and the northwest are observed (p.o. 5, 6, 7, 8). Near the p.o.5 there passes the zone of the large break having meridional strike. She is found on strong crushing of breeds and traces of a dry topping. The site is cut by also large zones of crushing and a bearing (**Table 1**).

The southern board of a canyon near a dam is characterized by prevalence of northeast and submeridional strike of the planes of cracks with falling of the planes to the West and the East.

Exposure is transverse by two large zones of crushing up to 0.3 - 0.5 m wide on dip Az 110˚ angle 65˚, 200˚/35˚ - 40˚. The planes of breaks are established visually. They prove in the form of several repeating series through 120 - 130

Table 1. The most widespread deformation elements of a northern shore.

Type	Dip azimuth/ angle
Large fissure	300˚/50˚, 290˚/60˚, 90˚/55˚, 80˚/50˚, 50˚/45˚, 120˚/50˚
Shatter zone (conditional plane)	p.o. 5 - 280˚/50˚, 130˚/65˚
Sliding mirrors on the large planes	p.o.5 - 305˚/45˚, 260˚/60˚ п.н.6 - 260˚/60˚, 215˚/75˚, 230˚/75˚
Dip fault	320˚ - 340˚/40˚ - 45˚
Upthrust	240˚ - 260˚/35˚ - 45˚

meters. The largest plane has elements: dip Az 90˚ angle 60˚. Width of a zone of crushing reaches 30 meters.

The zone of crushing of breeds alternates through 50 - 120 meters. Three such zones of crushing are found. Hypsometric lower the p.o. 5, is closer to a surface of the water, in the paleozoic breeds presented by lime sandstones small accurate dumping with left-side to shift components is observed (dip Az. 40˚ angle 65˚).

For studying of features of kinematics of boards of a reservoir measurements of elements of mirrors of sliding in local points have been executed and total values of "vectors" of motions for separate blocks are determined by the technique developed by the author [12]. It consists in definition of total "vector" (direction) of a motion of the tectonic block according to local data of separate points of observations. Such definitions are executed for the basis directly at the lower reach of a dam, a northern and southern board and also on some removal of the southern board of a reservoir. The obtained data are reflected in the **Figure 1**. Near a dam on the southern board of a canyon in the p.o. 1 and p.o. 2 "vectors" of shifts have orientation to the southwest. In the p.o. 1 orientation accurate, is localized strictly on an azimuth 250˚. In item 2 there is no such clearness, more along the subwidth axis and in N-W the sector is scattered. Approximately the same is found out in the item of 9 (**Figure 1**) though here the small confinedness of vectors to the subwidth direction and N-W to the sector is observed. In the item 3 prevails S-E the direction of vectors. The same picture is represented also in p.o. 5, 6, 8, 10.

In the dam basis at the lower reach cracks of S-W and N-W of falling prevail (the item of 9). In general the analysis of materials shows that near a dam strike of cracks tends north-east orientation when falling the planes to the southeast and the West (**Table 2**).

On the southern shore of a reservoir, in the p.o. 14 and 15, shifts of blocks are presented in the form of the upthrus-shifts and dip fault -shifts focused in the N-E, S-E direction. In item 15 dip fault -shifts prevail. The northern board near a dam is represented by p.o. 5 - 8, etc. In **Figure 1** it is visible that the northern site of the basis of a dam is displaced to the southeast. The southern site of the basis of a dam is displaced to the southwest. By detailed consideration it turns out that the line dividing multidirectional shifts has northwest strike, passes be-

Table 2. The most often met elements of deformations near a reservoir dam.

Type	Dip azimuth/anle
Large fissure	280˚ - 290˚, 335˚/55˚ - 60˚, 90˚.
Shatter zone (conditional plane)	280/50˚, 335˚/50˚, 60˚/60˚, 90˚/50˚
Sliding mirrors on the large planes	p.o. 9 - 10˚/70˚, 350˚/75˚ p.o.10 - 335˚/58˚, 335˚/55˚, 90˚/55˚
Dip fault	340˚/75˚, 335˚/60˚
Upthrust	p.o. 9 - 10˚/70˚, 350˚/75˚ p.o. 10 - 335˚/58˚, 335˚/55˚

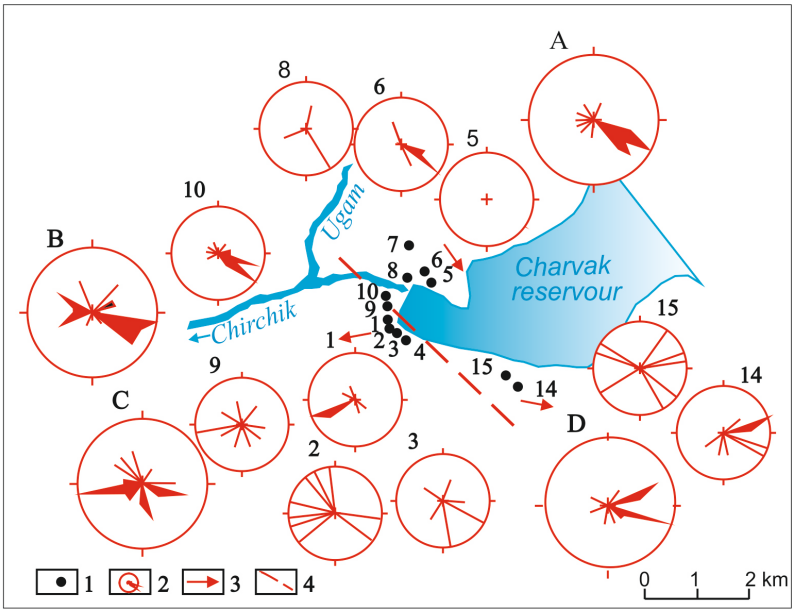

Legend: 1—points of observations; 2—roses-charts of the directions of motions on mirrors of slidings: are designated by figures for local volumes of points of observations, the letters A, B, C, D have designated total charts for the respective sites: A—northern, B—basis at the lower reach, C—southern, D—southern, on some removal from a dam; 3—direction of a total motion of the respective site; 4—conditional line dividing diverse directional blocks of the massif of rocks.

Figure 1. Roses of the directions of shifts of mountain masses in local volumes of points of observations and certain sites of a coastal zone of the Charvak reservoir according to geological observations.

tween p.o. 9 and p.o. 10 at the dam basis, p.o 4 and p.o. 14 and p.o. 15 located to the east (Figure 1). Noted line corresponds to strike of one of a branch of a Kumbel-Ugam series of breaks.

Together with motions of the tectonic nature in certain sites motions of another, perhaps, technogenic character is found. Detailed study of exposures of rocks of points of observations allows noting distinct expressiveness of separate fresh furrows of slidings. For example, in the p.o. 9 surfaces of sliding (dip Az. 10˚ anle 70˚, 350/75˚) upthrust type differs from other surfaces markedly (which are characterized by prevalence of large waste surfaces—dip Az.340˚ angle 75˚, dip Az 335˚ angle 60˚). In the p.o. 10 increases in number of the planes of slidings with dip Az 335˚ angle 58˚, 335˚/55˚, 90˚/55˚. The value of visible shift on them reaches 80 sm that unambiguously is established on outlines and the drawing of wings. Education of the last (judging by outlines) belongs by the time of laying of a dam (1971-1972). These data testify in favor of presence of fresh shifts of blocks of rocks in a coastal part of a reservoir. And shifts of trailing wings are directed towards a reservoir. Such feature of distribution of the planes with mirrors of sliding allows to assume that the lower parts of blocks of rocks, being under pressure, are deformed, being kind of pressed through under overlying layers.

On the basis of field tectonophysics survey of boards of the Charvak water reservoir in a structure of an array of rocks of boards of a water reservoir the larg-

est zones of explosive violations which form a step relief with different hypsometric situation the terrace of surfaces (Q_2) that testifies to youth of movements are selected.

Closer to an alignment of a dam a series of the explosive violations which are logging in the Kumbel-Ugam zone is fixed. In general two directions of extension of cracking are characteristic of all region of a water reservoir: 1) azimuth of extension 10˚ - 20˚ (190˚ - 200˚); 2) azimuth of extension 80˚ - 85˚ (260˚ - 265˚). Falling of the planes on the southeast prevails and, it is slightly less, on the northwest. On a section near a dam 4 directions of orientation of the planes of cracks are marked: one, more expressed (Az. strike 10˚ - 15˚), also rub less expressed (Az. strike 80˚, 320˚, 90˚). Are selected with the largest planes of crushing near a dam such as dip Az 280˚angle 50˚, 335˚/50˚, 60˚/60˚, 90˚/50˚. On deleting from a dam on the southern board the width extension with various falling prevails.

The following kinematic pattern is characteristic of boards of a reservoir. On a small section of the southern board of a canyon near a dam alignment vectors of offsets have orientation to the southwest. Northern board of a canyon experiences offsets preferentially to the southeast. In the southern board of a reservoir upthrus-shifts and dip fault-shifts have the direction on north-east and the southeast. On sections near a dam on northern and southern board of a canyon the increased frequency of occurrence of fresh mirrors of slidings is marked. Especially accurately they are shown at the lower reach of a dam on the planes: dip Az 335˚ angle 60˚, 90˚/55˚. In the majority of the planes of offset of trailing wings are directed towards a reservoir. The nature of residual deformations demonstrates that units of rocks of the lower part of a reservoir, are kind of pressed through under overlying breeds.

The analysis of all these data demonstrates that in the massif of rocks of boards of a reservoir there are active, rather young shifts of tectonic blocks. Connection of some of them with operation of a reservoir is supposed: the created external loading from a reservoir leads to redistribution of fields of tension of massifs of rocks of close located sites, or strengthening tectonic tension, or reducing them. It, in turn, strengthens deformation processes with the shift of tectonic blocks.

3.2. Studying of Kinematics and Dynamics of Blocks in the Mining Area

Similar researches have been conducted by us in the Almalyk mining district, on the square to the west from Urgaz (**Figure 2**). This area is in limits of northwest slopes of Kurama Ridge Tien Shan. Massifs of rocks are presented by paleozoic sedimentary, magmatic, volcanogenic and sedimentary formations of the lower and average carbon fabrics to a large extent, and in smaller—the lower perm. In a middle part of valleys of the rivers Almalyk Saukbulak in the width direction is stretched a large zone of the Burgundin break.

Closer to the southern part of the considered site in upper courses Kyzata and

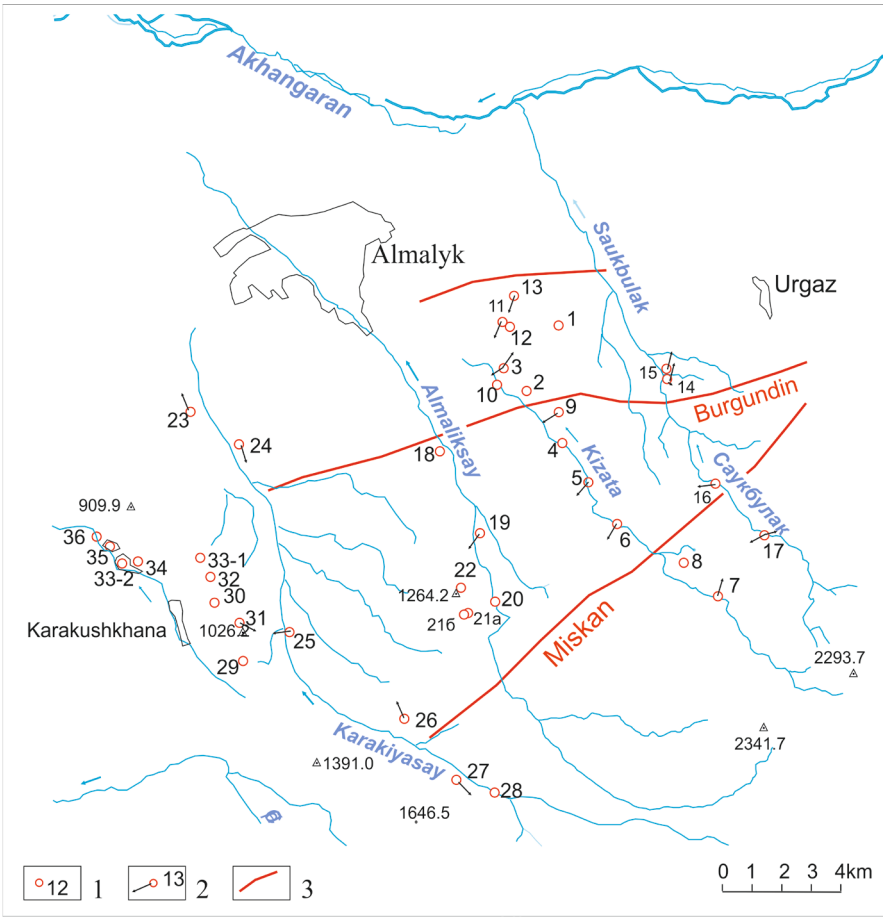

Legend: 1—points of observations of mirrors of sliding in the local volume of the massif of rocks; 2—primary directions of motions of local volumes on sliding mirrors; 3—main braking structures.

Figure 2. The directions of motions in local points of observations of the massif of rocks in the Almalyk mining district (The Kurama ridge, Tien Shan).

Saukbulak is stretched in the northeast direction a zone of the Miskan break. These breaks of ancient laying, have played an important role in formation of an overall picture of a geological structure. Some researchers consider that they have no activity in the latest time [12]. However, signs of expressiveness of a zone in a relief and some other new data demonstrate modern activity of these zones.

In each point of observation from 5 - 6 to 20 measurements of furrows of slidings are executed. Calculations and constructions are executed by the technique described in works [13] [14]. For each point of observation summary roses charts of the directions of shifts of blocks of rocks which participated in the subsequent when determining the directions of total motions of large volumes, the corresponding tectonic blocks are received.

In the central and northern part of the site of the direction of motions in local volumes are mainly focused on the southwest, and less often to the west. Such picture is observed in valleys of the Saukbulak and Kyzata Rivers. In the southern part of the site, in Kyzata and Karakiya courses there are points of observa-

tions in which the direction of motions changes on northeast. They are dated for the southern wing of the Miskan break that allows considering about manifestation of multidirectional motions of wings. Signs of left-side shift are noted. In a northern and northeast part of the site several local volumes with change of the directions of motions also on northeast are found. These points are on a northern wing of the width Burgundin break that can demonstrate manifestation of right-hand shift of wings. The Burgundin break is border of different types of structures—the northern part of the site which is a little raised represents a horst—the anticlinal structure called Kalmakyr, southern lowered, represents a graben-syncline structure called Central [12].

On the basis of the obtained data on shifts on sliding mirrors for each local volume of the massif of rocks charts of orientations of axes of the main normal tension have been constructed.

The circular chart A (**Figure 3**) is summary for all studied area and reflects distribution in Woolf's grid of points of an exit to the top hemisphere of axes of the main normal tension of compression, stretching and intermediate, points of observations received for local volumes. Axes of compression have meridional horizontal position, deviating to the northeast and the northwest. The stretching axis has vertical position more, being sometimes interchanged the position from intermediate. This chart confirms dynamic conditions when upthrus, upthrus-shift types of deformation elements are formed. This field of tension corresponds to the regional field of tension of the first rank which was received earlier and characteristic of all Chatkal-Kurama mountain area (**Figure 3(C)**). The general regional field of tension for western, Central Asian, parts of Tien Shan, received by us earlier according to geological data is characterized by the same type, but has northwest (southeast) orientation of an axis of compression (**Figure 3(B)**). The received picture of tension allows understanding kinematics and dynamics of the massif of the Almalyk district, in particular Entre Rios Saukbulak- Kyzata-Almalyk. They show that in the Central block shifts in southwest and partly in the western direction are noted. On the Burgundin break existence of right-hand moving is supposed. In the southern part of the site, in points located on different wings of the Miskany break confirm manifestation of left-side shift.

4. Conclusions

The analysis of the received materials allows drawing the following conclusions:

On the example of geological inspection of a coastal zone of the Charvak reservoir, the Almalyk mining area is shown the possibility of study of kinematics and dynamics of massifs of rocks of industrial regions.

The technique of reconstruction of fields of tension according to the kinematic analysis of structures of destruction in the conditions of an orogen of Tien Shan and the technique of kinematic reconstruction of motions of tectonic blocks according to local volumes of points of observations are tested. In massifs of rocks of a coastal zone of the Charvak reservoir presence of multidirectional shifts of boards, connected as with late Cenozoic tectonic processes, and tech-

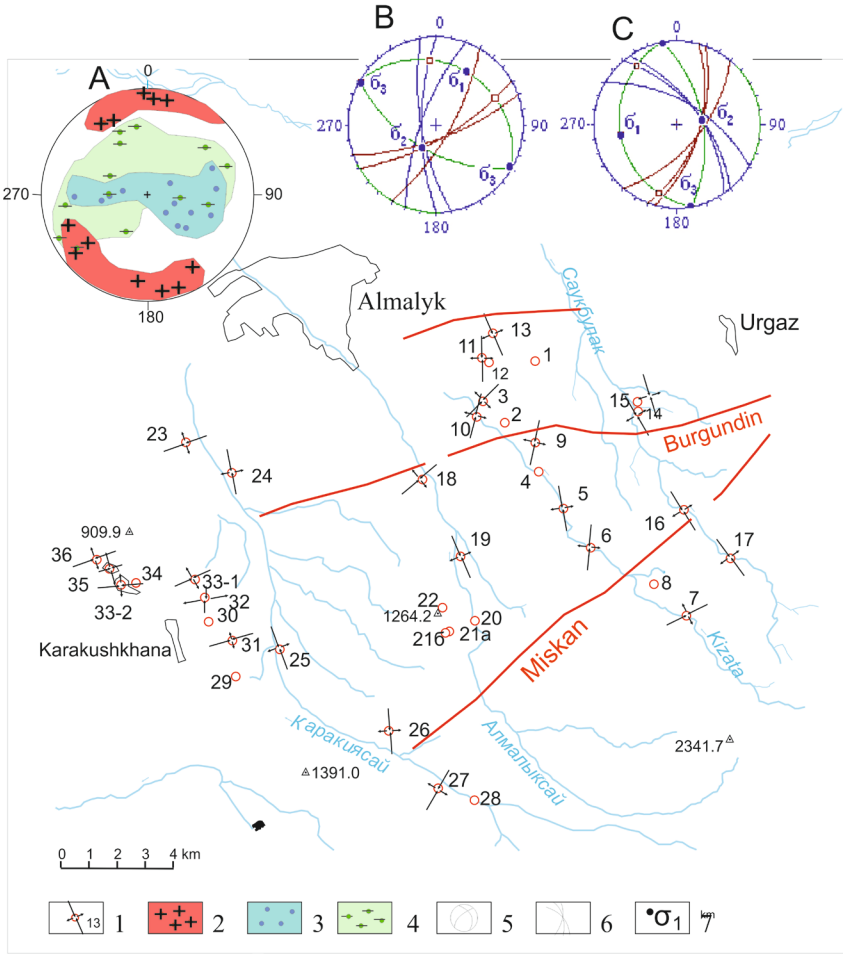

Legend: 1—orientations of axes of tension of compression and stretching in the corresponding local volumes of points of observations, 2 - 4—on the circular chart A: areas of points of an exit to the top hemisphere of axes of tension of compression (2), stretching (3) and intermediate (4); 5—circular charts received on Woolf's grid, the top hemisphere; 6—on the charts B and C: dispersion split of surfaces; 7—projections of points of an exit to the top hemisphere of axes of the main normal tension (compression-σ_1—stretchings, σ_2—intermediate, σ_3—compression).

Figure 3. The scheme of orientations of axes of the main normal tension in local volumes of points of observations and charts of axes of tension of the lowest ranks, generalized for different volumes, according to geological data (A—for the considered massif of rocks of the Almalyk district on sliding mirrors; B and C regional, according to the statistical analysis of jointing [9]: B—summary for the western part of Tien Shan, C—for Chatkal-Kurama mountain area).

nogenic factors are established.

In the industrial mining Almalyk region where intensive mining is carried out, contrast upthrus, upthrus-shifts with formation of the folded and block, shattered structure of massifs of rocks are observed. Observed shifts on mirrors of sliding have allowed reconstruction of the field of tension of the Almalyk district which is characterized by horizontal, submeridional orientation of an axis of the main normal tension of compression, at inclined position of two others. It corresponds to the field of tension of the first rank for Chatkalo-Kurama mountain area and defines the general dynamic conditions of the area. To Entre Rios

Saukbulak-Kyzata-Almalyk, in the Central block are noted shifts in southwest and partly in the western direction. On the Burgundin break presence of right-hand shift is noted. In the southern part of the site, on different wings of the Miskan break are noted left-side moving. Such kinematics on breaks is caused by operation of the specified blocks of the squeezing efforts of submeridional orientation, external on the relation.

On studying dynamics of massifs of rocks are usually carried out by tool methods of measurement of pressure on small sites, directly in excavations. The difficult relief and tectonics don't allow carrying out them on big squares. From materials of this article it is visible that for studying of dynamics of massifs of rocks by geological methods it is possible to capture big sites. Besides, the genetic linkage of the obtained data with the general tendency of geodynamic development of the studied region is defined.

Thus, the received results testify to a possibility of receiving by geological, namely field tectonophysics methods of important data on kinematics and dynamics of massifs of rocks, tectonic blocks, and features of their deformation. Such studying of the massif of rocks before the beginning and in the course of performance of work on mining is important for the choice of design and optimum parameters of laying of excavations, control of a condition of their boards and walls, definition of strategy of safety of conducting mining operations and also seismic stability of constructions.

References

[1] Angelier, J. (1979) Determination of the Mean Principal Stress from a Given Fault Population. *Tectonophysics*, **56**, T17-T26. https://doi.org/10.1016/0040-1951(79)90081-7

[2] Angelier, J. and Baruah, S. (2009) Seismotectonics in Northeast India: A Stress Analysis of Focal Mechanism Solutions of Earthquakes and Its Kinematic Implications. http://lib.icimod.org/record/9325 https://doi.org/10.1111/j.1365-246X.2009.04107.x

[3] Gushenko, O.I. (1979) Method of the Kinematic Analysis of Structures of Destruction at Reconstruction of Fields of Tectonic Tension. Weeding of Tension and Deformations in a Lithosphere. Collection of Scientific Works. Science, Nauka, Moskow, 7-25. (In Russian)

[4] Sim, L.A. (2013) Overview of the State of Knowledge on Paleotectonic Stresses and Their Implications for Solution of Geological Problems. *Geodynamics* & *Tectonophysics*, **4**, 341-361. (in Russian)

[5] Umurzakov, R.A. (2012) Late Cenozoic Tectonic Stresses and Focal Mechanism of Some of the Largest Earthquakes of the Tien Shan Region. *Comptes Rendus Geoscience*, **344**, 239-246. https://doi.org/10.1016/j.crte.2012.03.003

[6] Rakhimov, V.R. and Chunikhin, S.G. (2008) Prospects of Development of Mineral Raw Material Resources of the Almalyk Ore Field. *Mountain Bulletin of Uzbekistan*, No. 2, 85-88. (In Russian)

[7] Dehnoo, E.N., Mirzeynali, H. and Farrokhnia, A. (2015) Analysis of Geomechanical Properties in Terms of Parametric Discontinuities on Stability of Tunnels Distinct Element Method (Case Study: Water Tunnel of Golab). *Open Journal of Geology*, **5**,

92-105. https://doi.org/10.4236/ojg.2015.53009

[8] Shanov, S. and Kostov, K. (2015) Dinamic Tectonic and Karst. XI. 123. http://www.springer.com/978-3-662-43991-3

[9] Smaglichenko, A.V., Sim, L.A. and Gorbatikov, A.V. (2014) A Complexity of the Displacement along Segments of the Akhtyirsk Fault//Emergency, Complexity, Computations. Book Series. Springer Publisher, Verlag Berlin Heidelberg, **8**, 395-400.

[10] Nikolaev, P.N. (1992) Methods of the Tectonodynamic Analysis. *Science*, Nauka, Moskow, 340. (In Russian)

[11] Umurzakov, R.A. (2008) Fields of Tension and the Mechanism of Formation of the Centers of Earthquakes in Some Mountain Areas of Tien Shan according to Geological and Structural Data. Tectonophysics and Topical Issues of Sciences about Earth. *Materials of Reports of the Russian Conference*, Moscow, 13-17 October 2008, 408-1110. (In Russian)

[12] Umurzakov, R.A. (2004) Technique and Some Results of Kinematic Reconstruction of Regional Late Cainozoic Shifts of Tectonic Blocks/Relief Generating Processes: Theory, Practice, Research Methods: Materials XXYIII of the Plenum of the Geomorphological Commission. Novosibirsk, 20-24 September 2004, 267-268. (In Russian)

[13] Yakubov, D.H. (1970) Breaks of Southwest Part of the Kurama Ridge. Fan, Tashkent, 184. (In Russian)

[14] Pharmanov, A.K., Sanakulov, K.S. and Shemetov, P.A. (2010) A State and the Prospects of Extraction of Precious and Non-Ferrous Metals in Uzbekistan. *The Mountain Bulletin of Uzbekistan*, No. 4. 44-48. (In Russian)

Scientific Research Publishing

World Journal of Mechanics, 2017, 7, 255-270
http://www.scirp.org/journal/wjm
ISSN Online: 2160-0503
ISSN Print: 2160-049X

Computational Analysis of the Metal Free-Surface Instability, Fragmentation, and Ejecta under Shock

Jingsong Bai[1,2], Tao Wang[1*], Jiaxin Xiao[1], Bing Wang[1], Han Chen[1], Lei Du[1], Xinzhu Li[1,2], Qiang Wu[1,2]

[1]Institute of Fluids Physics, China Academy of Engineering Physics, Mianyang, China
[2]National Key Laboratory of Shock Wave and Detonation Physics (LSD), Institute of Fluid Physics, China Academy of Engineering Physics, Mianyang, China
Email: *wtao_wyn@foxmail.com

How to cite this paper: Bai, J.S., Wang, T., Xiao, J.X., Wang, B., Chen, H., Du, L., Li, X.Z. and Wu, Q. (2017) Computational Analysis of the Metal Free-Surface Instability, Fragmentation, and Ejecta under Shock. *World Journal of Mechanics*, **7**, 255-270.
https://doi.org/10.4236/wjm.2017.79021

Received: July 14, 2017
Accepted: September 12, 2017
Published: September 25, 2017

Abstract

We conducted numerical simulations of the related processes of interface instability, tensile fragmentation, and jetting resulting from four kinds of typical macro defect perturbations (chevron, sine wave, rectangle, and square) on a Cu free surface under a reflected shock wave when Cu impacts a solid wall at a speed of 2.5 km/s and found that, for the chevron and sine wave cases, the ejecta velocities of the head are 6.28 and 5.88 km/s, respectively. Some parts of the inner material are in a tensile state without any fragmentation, which is observed only in the main body of the material owing to the tension effect. Furthermore, for the other two initial perturbations (rectangle and square), the highest ejecta velocities may even reach 9.14 and 9.59 km/s, respectively. Fragmentation caused by multilayer spallation can be observed on a large scale in the Cu main body, and there are granules in the front area of the ejecta but the degree to which fragmentation occurs is much less in the Cu main body and there is a notable high-speed, low-density granule area in the ejecta head. Finally, we present a detailed analysis of the spatial distribution of the granules, ejecta mass, pressure, temperature, and grid convergence.

Keywords

Interface Instability, Particle Ejecta, High-Speed Collision, Spallation

1. Introduction

Metal interface instability occurs as a reaction to the effect of a shock wave or acceleration or to a shear load on the perturbed interface, and may afterward

lead to fragmentation and mixing. This phenomenon, common in explosions and shock processes under extreme conditions (high temperature and high pressure), is jointly controlled by three scale factors, *i.e.*, 1) the thermodynamics and the geometric boundary (macroscopic scale), 2) the initial perturbation of the metal interface (mesoscopic scale), and 3) material properties (microscopic-mesoscopic scale). Metal interface instability is a typical multiscale, multiphysical, strongly coupled, nonequilibrium, and complex flow phenomena.

Related studies of the Rayleigh-Taylor (RT) instability of metal began in the 1970s. In particular, in the USA and Russia, theoretical studies, numerical simulations, and experimental investigations have been conducted. The prior research by Barnes, Blewett, McQueen, Meyer, and Venable [1] mainly focused on the metal interface instability growth of a flat plate driven by expansion of detonation products, as observed in the Los Alamos high-energy X-ray facility. By modeling with the two-dimensional elastic-plastic numerical hydrodynamics code MAGEE, they confirmed that amplitude growth was apparently governed mainly by the dynamic yield strength of the material. This pioneering experiment has been regarded as the standard experimental model in solid RT instability research. To confirm the theoretical analysis of Drucker [2], the additional experiments conducted by Barnes, Janney, and London *et al.* [3] showed that no more than semiquantitative agreement can be expected between the experiments and the results. However, the main conclusion reached by Drucker [2], that amplitude and wavelength determine the onset of the RT instability in a solid, has been proved in the experiments. Nevertheless, since Barnes, Blewett, McQueen, Meyer, and Venable's research [1], which was limited by the testing and diagnostic techniques, related experiments on the RT instability in a solid have not been improved by much. In 2006, Lindquist, Cavallo, and Lorenz *et al.* [4] studied the metal RT instability under high pressure and high strain rate, utilizing the same experimental configuration as did Barnes, and combining with numerical simulation, they eventually confirmed the applicability of the standard constitutive models: Steinberg Guinan (SG) and Preston-Tonks-Wallace (PTW). In recent years, owing to the rapid development of laser equipment and the construction of large laser-loaded devices, related laser-loaded experiments have been conducted. To study the effect of material strength on the metal RT instability under Mbar pressure, Weber, Kalantar, and Colvin *et al.* [5] have conducted a hohlraum experiment of an X-ray-driven metal layer using NOVA. Because of the X-ray preheating and metal-melting problem, these experiments failed to provide any definitive results. To eliminate the effect of preheating and metal melting, Edwards, Lorenz, and Remington *et al.* [6] developed a new laser-driven method for dynamic shockless loading of solid materials. Based on this platform, Lorenz, Edwards, and Jankowski *et al.* [7] [8] used the Omega laser to research metal RT instability under high pressure and high strain rate. In 2009, Park, Remington, and Beckeret *et al.* [9] also utilized the Omega laser to study RT instability under Mbar pressure. In their experiment, the target samples were driven quasi-isentropically. To solve the problems resulting from preheating and

metal melting, plasma from a laser-driven polymer layers acts on the CH-based epoxy samples across the vacuum gap. In 2014, Smalyuk, Casey, and Clark *et al.* [10] firstly observed the hydrodynamic instability growth in indirectly driven implosions at the National Ignition Facility; their results are in good agreement with theoretical and simulation studies. Their work is the first step in experimentally studying hydrodynamic instability in a converging configuration. American and Russian researchers [11] [12] [13] conducted explosive and magnetic driving experiments to research material constitutive behavior by using perturbation growth and then developed a new material constitutive model to predict the results of experiments under high pressure and high strain rate. In the 1990s, using a high-speed camera, Chen, Zeng, and Wang *et al.* [14] performed experimental research on the interface instability of a alloy/water system in a cylindrical implosion configuration that was numerically simulated based on the hydrodynamics by Lin, Xia, and Zhang [15]. Recently, Wang, Bai, and Cao *et al.* [16] have conducted experiments and numerical simulations of an aluminum flyer driven by an explosion and observed the sine perturbation growth at early time.

The theoretical study of the metal RT instability is limited by the material models used and also the lack of comparison with related experiments. Particularly, at the turbulent mixing stage, it is difficult to predict the development of the interface instability. Despite some progress made in experimental studies, understanding of metal instability in detail is still hindered by diagnostic techniques. Therefore, because the problems in algorithm precision, the constitutive model, and the equation of state (EOS) are still too tough to solve, simulation work stands out as especially worthwhile. Some effective software and codes, such as ABQUS, Lagrange codes FCI2, MAGEE, TOODY II [17], and Euler codes ALE3D and CHAP [18] and the two-dimensional (2D) Euler MHD program, have been designed and improved just for this purpose. By combining simulation and experiment, the evolution pattern of the metal interface instability is presented with time. The instability growth obtained indicates that the material strength and load history and the perturbation wavelength and amplitude have a vital influence on the RT instability. Specifically, the material strength restrains the growth and development of the interface instability, and only when the initial amplitude reaches or exceeds a specific value does the instability develop.

Under shock loading, macro defects perturbations on metal free surface may lead to ejecta and fragmentation. We numerically studied the growth of the instability on the metal interface with four kinds of typical macro defect (chevron, sine wave, rectangle, and square) perturbations and the dynamic characteristics of ejecta.

2. Numerical Methods

Given a multimaterial, large-deformation, strong-shock physics problem, we improved our previous large eddy simulation code MVFT (multiviscous flow

and turbulence) [19] [20] [21] by taking into consideration explosive detonation and the elastic-plastic behavior of the material. An Euler finite volume algorithm and code describing detonations and shocks dynamics with three-order accuracy has been developed using the two-step Euler algorithm with three-order accuracy. More specifically, the Lagrange and remap algorithms are applied to solve the mass, momentum, and energy conservation equations. In a single Lagrange step, the integration of the Lagrange control equation at one time step is obtained, the deformation of the material leads to deformation of the initial grid, and there is no material flow between the grids, whereas, in a single remapping step, the velocity and energy, deviation stress, and other state parameters in the Lagrange deforming grid are remapped back to the initial grid. The governing equations used are given as follows:

$$\begin{aligned}
&\frac{\partial}{\partial t}\int_V \rho \mathrm{d}V = -\oint_S \rho u_i n_i \mathrm{d}S,\\
&\frac{\partial}{\partial t}\int_V \rho u_j \mathrm{d}V = -\oint_S P n_j \mathrm{d}S + \oint_S s_{ij} n_i \mathrm{d}S - \oint_S \rho u_i u_j n_i \mathrm{d}S,\\
&\frac{\partial}{\partial t}\int_V \rho E \mathrm{d}V = -\oint_S u_j P n_j \mathrm{d}S + \oint_S u_i s_{ij} u_j \mathrm{d}S - \oint_S \rho u_j E n_j \mathrm{d}S,
\end{aligned} \tag{1}$$

where V is the control volume, u_j is the velocity, S is the surface area of control volume, $\vec{n}$ is the external normal line, s_{ij} is the deviatoric stress tensor, P is the static pressure, and E is the total energy per unit mass.

First, in our numerical simulation, a dimension splitting method is used to split Equation (1) into three one-dimensional problems, which are then solved using the piecewise parabolic method (PPM) method to perform the interpolation and reconstruction of the physical quantity in each grid. Owing to the lack of automatic monotonicity of PPM, there would be numerical oscillation at the discontinuity point, which leads to a decrease in the accuracy of the discontinuous solution. To restrict the numerical oscillation, we introduce a flow restrictor. In adopting this method, a monotonic limiter is utilized so that the calculation of δQ_j is limited monotonically, as shown in the following:

$$\left(\delta Q_j\right)_{mono} = \begin{cases} \min\left(\left|\delta Q_j\right|, 2\left|Q_j^n - Q_{j-1}^n\right|, 2\left|Q_{j+1}^n - Q_j^n\right|\right)\mathrm{sgn}\left(\delta Q_j\right), & \left(Q_{j+1}^n - Q_j^n\right)\left(Q_j^n - Q_{j-1}^n\right) > 0, \\ 0, & \left(Q_{j+1}^n - Q_j^n\right)\left(Q_j^n - Q_{j-1}^n\right) \le 0, \end{cases} \tag{2}$$

to keep $Q_{j+1/2}^n$ between Q_j^n and Q_{j+1}^n, where the Q are conservation quantities.

In a Lagrange step, the material strength model, artificial viscosity, and explosive detonation model are needed for calculation and, therefore, the Jones-Wilkins-Lee (JWL) equation of state is used for the explosive detonation and the Mie-Gruneisen equation of state is applied for the strength material. As for the strength model, we utilize the Steinberg-Guinan constitutive model.

In the Steinberg-Guinan constitutive model [22], terms for pressure, temperature, and strain rate are added to the elastic-plastic constitutive equation while the coupling effect of pressure and strain rate on flow stress has a characteristics

of separating variables. Additionally, because the flow stress in the Steinberg-Guinan constitutive model relies on pressure, the material constitutive equation and the state equation are coupled, indicating stress hardening of the metal under a high pressure. The shear modulus and flow stress in the Steinberg-Guinan constitutive model can be expressed as

$$G(P,T) = G_0\left[1+\frac{1}{G_0}\left(\frac{\partial G}{\partial P}\right)_0 \eta^{-1/3}P + \frac{1}{G_0}\left(\frac{\partial G}{\partial T}\right)_0 (T-300)\right], \tag{3}$$

$$\sigma_{SG} = Y_0\left(1+B\varepsilon\right)^n\left[1+A\eta^{-1/3}P-\alpha(T-300)\right], \tag{4}$$

where Y_0 signifies the yield strength in the initial state, G_0 is the shear modulus in the initial state, P and T are the pressure and temperature, $(\partial G/\partial P)_0$ and $(\partial G/\partial T)_0$ represent, respectively, the partial derivatives of shear modulus to the pressure and temperature in the initial state, A and α correspond to $(\partial G/\partial P)_0/G_0$ and $(\partial G/\partial T)_0/G_0$, B and n are material strain hardening parameters, ε is the strain, and $\eta = \rho/\rho_0$ is the material compression ratio.

The form taken by the Steinberg-Guinan constitutive model is irrelevant to the strain rate, yet the requirement upon the strain rate is that it should be $>10^5$ s^{-1}. The reason for this restriction is that the effect of metal softening counteracts that of metal hardening, so this model can be used to describe multimaterial flow stress under high pressure, which is also the mostly used constitutive model under high pressure.

3. Validation of the Simulation Code

Through simulation of Barnes's three experiments [1] [3] on an 1100-0 Al flat plate accelerated by a detonation product, we confirmed the simulating capability of the high-fidelity detonation and shock dynamics calculation program. In these experiments, the initial perturbations of the Al flat plate were 1) initial wavelength 5.08 cm and initial amplitude 0.02 cm, 2) initial wavelength 2.54 cm and initial amplitude 0.01 cm, and 3) initial wavelength 4.8 cm and initial amplitude 0.01 cm. They utilized a P80 detonation plane-wave lens to trigger a shock initiation on a 3.81-cm-thick PBX-9404, after which the detonation products form an isentropic load for the Al plate through a vacuum gap 2.54 cm long. The parameters of the PBX-9404 JWL EOS used in the simulation are given in **Table 1**. The 1100-0 Al Mie-Gruneisen EOS and Steinberg-Guinan constitutive model parameters are listed in **Table 2** and **Table 3**.

In the first experiment (wavelength 5.08 cm and amplitude 0.02 cm), it can be seen that, by a seminumerical linear analysis, when Y_0 = 0.055 GPa, the numerical simulation agreed well with the experiment data. Although the 2D calculations of our program agree well with the experiment (Y_0 = 0.075 GPa), there are differences between the above results and those from the 1100-0 Al Steinberg-Guinan constitutive model under the condition of Y_0 = 0.04 GPa. This is true especially when Y_0 = (0.325 GPa) and (0.2 GPa), in which case the results significantly differ from those in ref. [1] [23], shown in **Figure 1**.

Table 1. PBX-9404 JWL EOS parameters.

ρ_0 (g/cm^3)	A (Mbar)	B (Mbar)	R_1	R_2	ω	E_0 (Mbar)	D_{cj} (km/s)
1.84	8.524	0.1802	4.6	1.3	0.38	0.102	8.8

Table 2. 1100-0 Al Mie-Gruneisen EOS parameters.

ρ_0 (g/cm^3)	c (km/s)	γ_0 (Mbar)	a	S_1	S_2	S_3
2.707	5.25	1.97	0.47	1.37	0.0	0.0

Table 3. 1100-0 Al Steinberg-Guinan constitutive model parameters.

G_0 (GPa)	Y_0 (GPa)	Y_{max} (GPa)	B	n	A (GPa^{-1})	α (kK^{-1})
27.1	0.04	0.48	400.0	0.27	0.0652	0.616

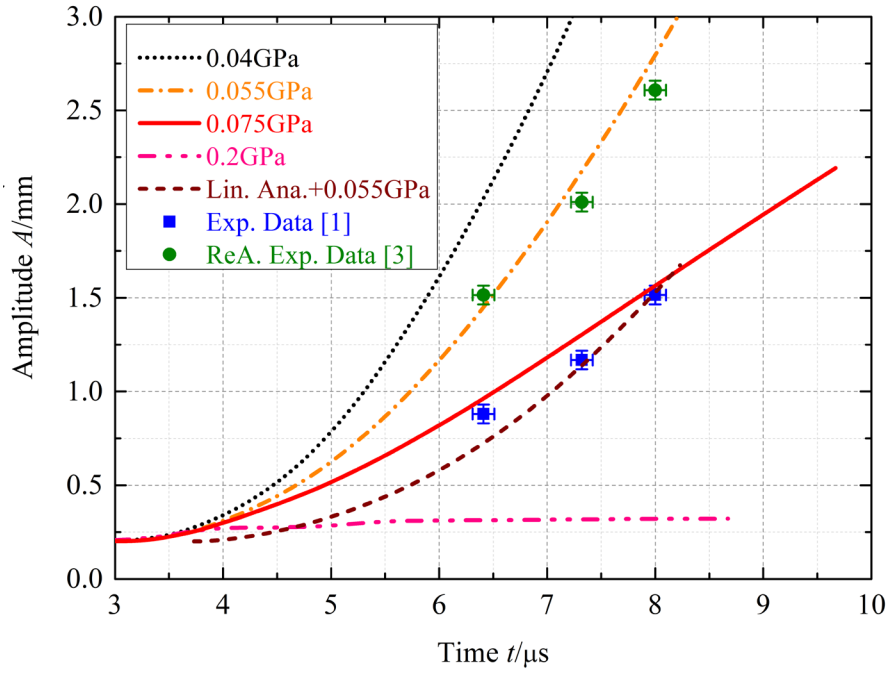

Figure 1. Experimental and numerical simulation amplitudes when the initial amplitude is 0.02 cm and the wavelength is 5.08 cm.

It is easily observed from **Figure 1** that the amplitude is almost a constant owing to the large strength. When Y_0 declines to 0.04 GPa, the growth of the amplitude calculated by our program is greater than that in the experiment, which indicates that the influence of the strength on the amplitude growth is weak. For the case when Y_0 = 0.075 GPa, the simulation result agrees well with that from the experiment. However, the result for Y_0 = 0.055 GPa coincides with Barnes's further analytical results, which took account of the deviation of X-ray photographic magnification [3]. Given the uncertainty deviation of the experiments, it is impossible to obtain a precise result for the initial yield strength by the comparison of numerical simulation and experiment. Nevertheless, the proper initial yield strength obtained from the simulation is supposed to illu-

strate the applicability of the constitutive model.

For the other two experiments, we conducted the simulation based on the initial yield strength Y_0 = 0.075 GPa of 1100-0 Al calibrated by using our program. In the simulation of the experiment (with wavelength 2.54 cm and amplitude 0.01 cm), three kinds of grid resolution were adopted: $\Delta x = \Delta y = 4$, 8, and 15 μm. In Figure 2, simulation results are seen to agree well with experimental results and show grid convergence. The simulation results in Figure 3 (with wavelength 4.8 cm and amplitude 0.01 cm) indicate the obvious convergence trend.

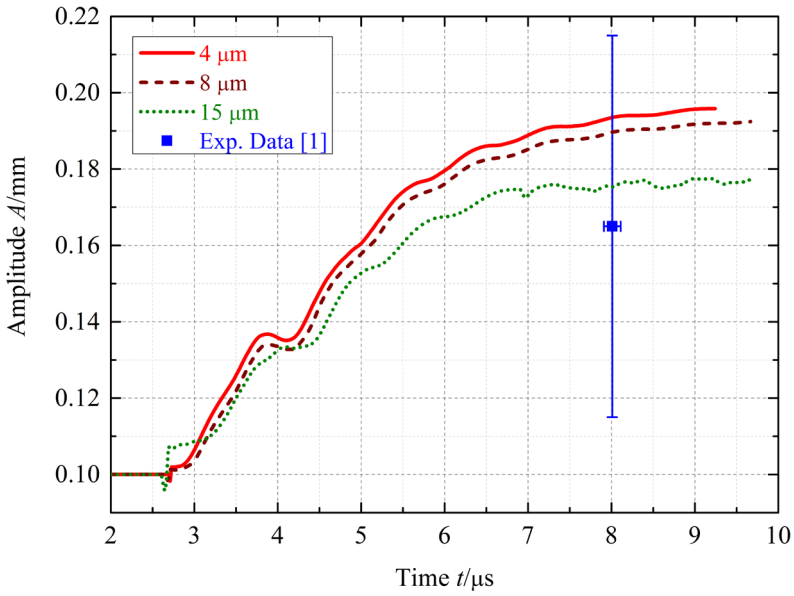

Figure 2. Experimental and numerical simulation amplitudes when the initial amplitude is 0.01 cm and the wavelength is 2.54 cm.

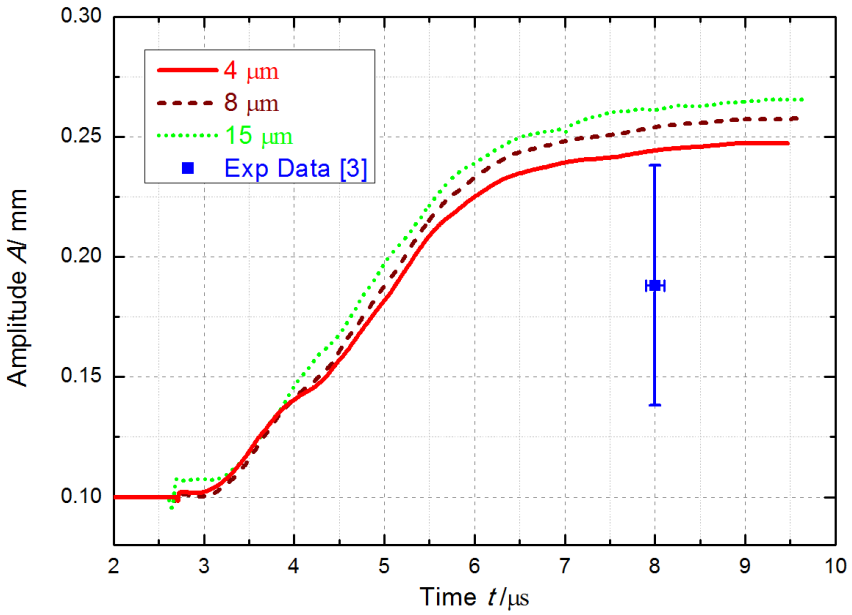

Figure 3. Experimental and numerical simulation amplitudes when the initial amplitude is 0.01 cm and the wavelength is 4.8 cm.

In summary, when the experimental conditions are $P \approx 10\,\text{GPa}$ and $\dot{\varepsilon} \le 10^5\ \text{s}^{-1}$, our calculation is in accordance with the experiment, and the grid convergence is also in the same trend.

4. Results and Discussion

Figure 4 shows the four kinds of typical macro defect perturbations (chevron, sine wave, rectangle, and square) on a Cu metal free surface under the reflected shock wave produced from copper impacting the left solid wall at a high speed of 2.5 km/s. When the reflected shock waves reach the free surface, the reflected rarefaction wave in the material leads to the acceleration of the interface particles, as well as to tensile and unloading effects. At the same time, various tensile failures in the material are also under complex and interacting influences of the solid wall's reflected shock wave and rarefaction wave. Owing to the different initial perturbations on the interface, $\nabla p \times \nabla \rho \neq 0$ results in the interface instability, fragmentation, and jetting. Numerical simulations are used to analyze quantitatively the difference in interface instability for four typical macro defects and to study the various distributing features of fragmentation and ejecta inside the material and around the interface. In our simulations, the Cu EOS and constitutive model parameters are given in Table 4 and Table 5.

Configuration of the calculation modes are shown in Figure 4; the computational domain is [0 cm, 8 cm] × [−1 cm, 1 cm], the length of Cu is 5 cm, and the boundary conditions on the left, top, and bottom edges are all the solid walls. The positions of the four defects (chevron, sine wave, rectangle, and square) are located at the center of the free surface, with the same area of 0.25 cm^2, and the Cu mass of defect unit thickness is 2.1 g. For the chevron, the defect shape is an isosceles right-angled triangle with a 1-cm-long bottom edge. The sine wave amplitude and wavelength are 0.3927 and 2 cm, respectively. Additionally, the length and width of the rectangle are 0.7071 and 0.35355 cm, and the length of the square is 0.5 cm.

To verify grid convergence, we take the chevron model as an example and select two different sizes (25 and 12.5 μm). Figure 5(a) and Figure 5(b) demonstrate the grid convergence of the velocity history of the interface vertex and the velocity distribution on the symmetrical axis at t = 13.5 μs. For the coarse and fine grids, the peak velocities are 6.32 and 6.28 km/s, the starting times of the vertex are 5.845 and 5.854 μs, and the relative errors satisfying the convergence

Table 4. Cu Mie-Gruneisen EOS parameters.

ρ_0 (g/cm^3)	c (km/s)	γ_0 (Mbar)	a	S_1	S_2	S_3
8.93	3.94	1.99	0.47	1.489	0.0	0.0

Table 5. Cu Steinberg-Guinan constitutive model parameters.

G_0 (GPa)	Y_0 (GPa)	Y_{max} (GPa)	B	n	A (GPa^{-1})	α (kK^{-1})
47.7	0.12	0.64	36.0	0.45	0.0283	0.377

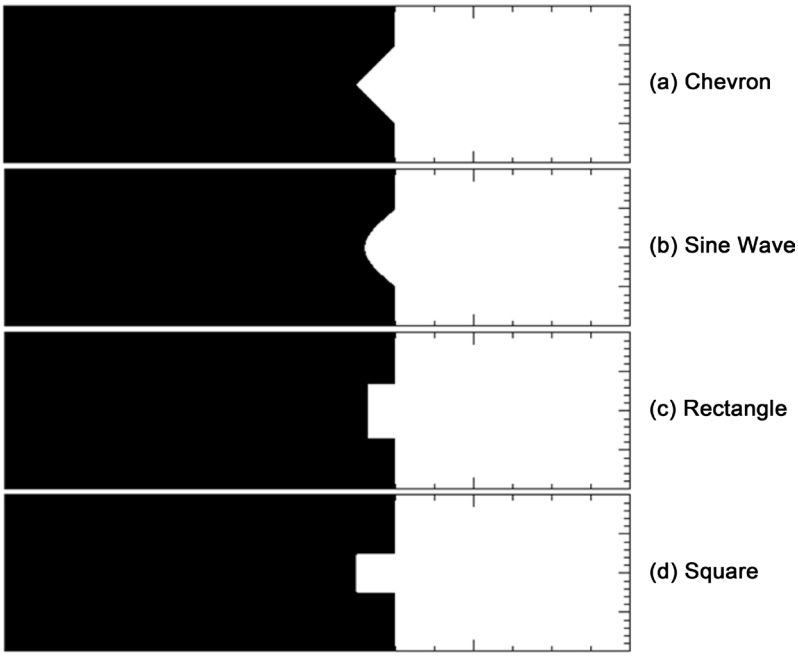

Figure 4. Four typical initial macro defects (chevron, sine wave, rectangle, and square) on the Cu free surface.

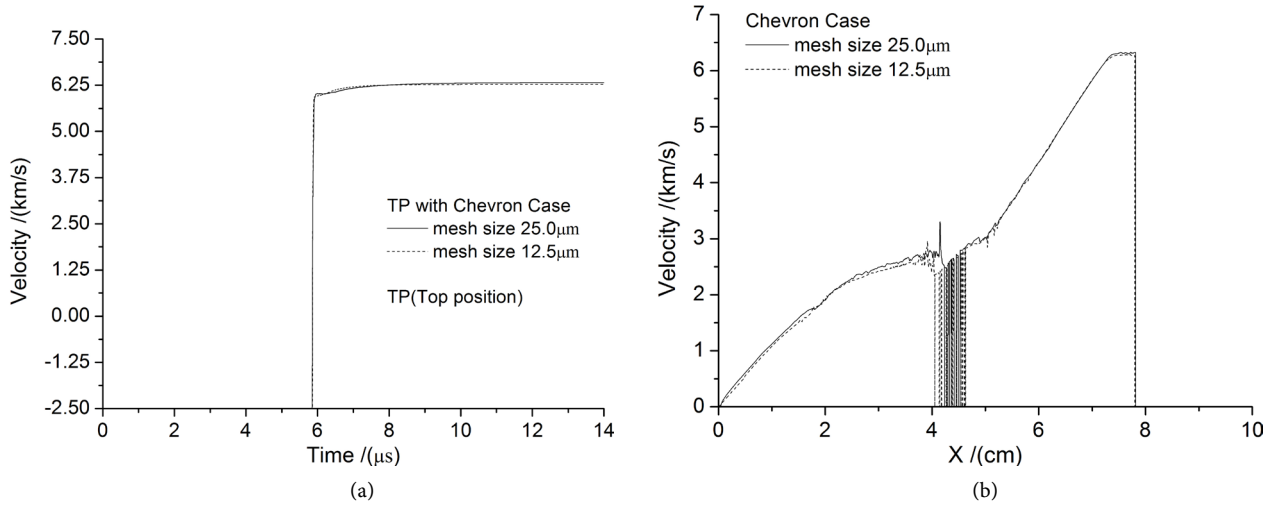

Figure 5. (a) Vertex velocity history of the chevron interface; (b) velocity distribution on the asymmetrical axis at $t = 13.5$ μs.

condition are 0.64% and 0.15%, respectively. In **Figure 5(b)**, it is obvious that the velocity distributions in the calculation area mostly satisfy the convergence condition, whereas the calculations of the quantity in the fragmentation area on the 4 to 5 cm horizontal axis display significant differences.

The left panel of **Figure 6** shows a partially enlarged view of **Figure 5(b)**, from which the size of the fragmentation area can be obtained. The width of the fragmentation area for coarse grid is 2.925 mm, and that in the fine grid is clearly larger (5.812 mm), which means that the size of the fragmentation area is related to the computational grid. Moreover, the size of the fragment is also easy to determine from that of the velocity discontinuity's discrete space. The size of the

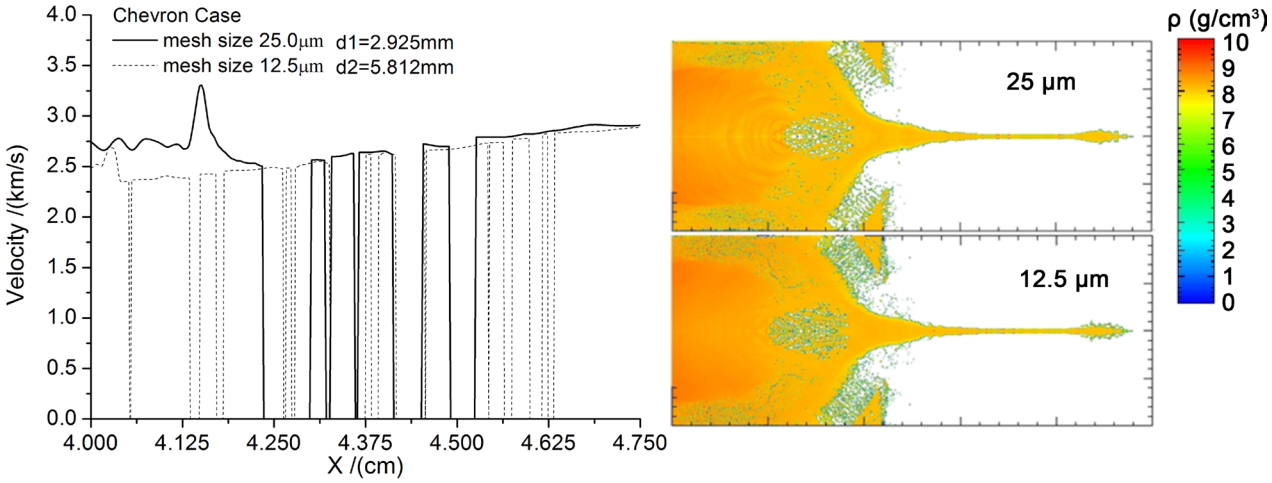

Figure 6. (Left) velocity distribution on the symmetrical axis of the chevron interface and (Right) density contour for a domain of [3 cm, 8 cm] × [−1 cm, 1 cm] at t = 13.5 μs.

large fragments is almost the same in the two different grids, and that of the smallest fragment even reaches one grid size, so the size of the smallest fragment is linked to the computational grid. The right panel of Figure 6, in contrast, shows the allelic distributions of the density in the coarse and fine grids at t = 13.5 μs, so the ejecta mass can be calculated (with the length of the horizontal axis exceeding 5.4 cm). Specifically, the ejecta masses are 0.799 and 0.737 g, respectively, and the difference is about 8.41%, suggesting that the ejecta mass is also closely linked to the computational grid.

The above findings reveal that the numerical calculations of the fragmentation are related to the size of the calculation grid. To eliminate the influence of the grid's mesh, we chose the same grid size, 12.5 μm in length, in the four models. Thus, the Euler mesh encompasses 12,800,000 points in the whole computational domain [0 cm, 10 cm] × [−1 cm, 1 cm].

To compare the various characteristics of the interface instability, fragmentation, and ejecta under the influence of the four typical defects, Figure 7 shows the material distribution at two moments (t = 10.5 and 13.5 μs), where the chevron ejecta shape is a nonuniform pole with a sharp-pointed nose. For the sine wave, the ejecta is also a nonuniform pole but with a mushroom head. The common characteristic in the former conditions is that hardly any distinct particle jet can be found. For the rectangle and square defects, the shared characteristic is that high-speed particles concentrate on the symmetrical axis of the ejecta head while they differ in that the rectangle has a conical hole shape in the front and the square is shaped like a large-size arc.

Table 6 lists the ejecta mass of the four defects when t = 10.5 and 13.5 μs. At 10.5 and 13.5 μs, the horizontal axis of the calculation domain is larger than 4.5 and 5.4 cm, respectively. From Table 6 we find that the ejecta mass of the chevron is 0.533 g, and those of the sine wave, rectangle, and square are, respectively, 0.581, 0.662, and 0.586 g. At t = 13.5 μs, the ejecta mass of the chevron is 0.737 g, and for cases the sine wave, rectangle, and square the ejecta masses are

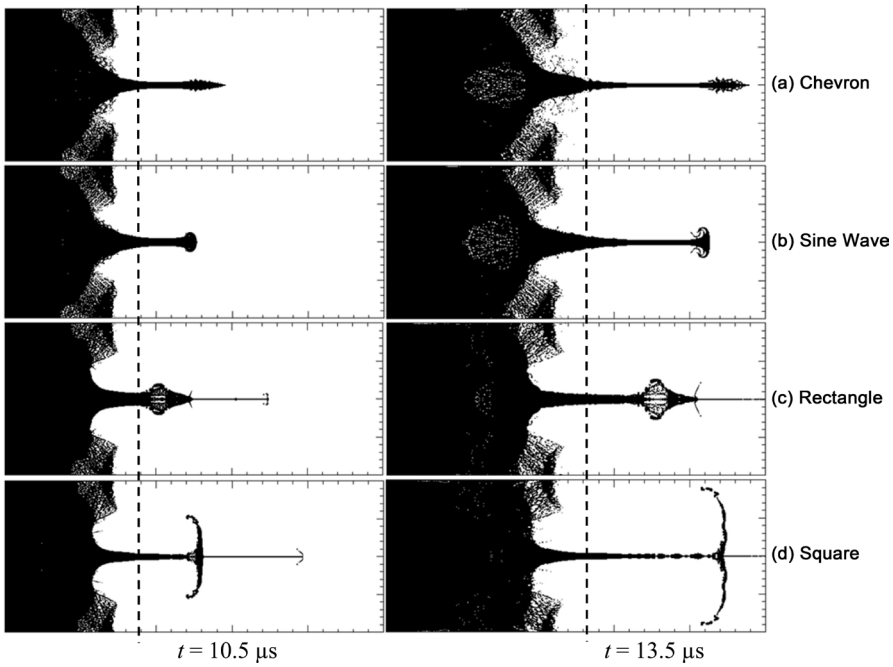

Figure 7. Calculated configurations of free surface instability, fragmentation, and the ejecta for the four defects at t = 10.5 and 13.5 μs: (a) chevron; (b) sine wave; (c) rectangle; and (d) square. The domain is [3 cm, 8 cm] × [−1 cm, 1 cm].

Table 6. Jet mass under the four defects at 10.5 and 13.5 μs.

Time (μs)	Ejecta mass (g)			
	Chevron	Sine wave	Rectangle	Square
10.5	0.533	0.581	0.662	0.586
13.5	0.737	0.803	0.848	0.712

0.803, 0.848, and 0.712 g, respectively. In summary, although all the ejecta masses increase with time, it is obvious that the law of ejecta mass and growth varies according to the kind of typical macro defect perturbation. The left panel of Figure 7 illustrates that the distributions of the fragmentation area near the interface located on both sides of the ejecta are basically the same, both being caused by the unloading of the free surface. Nevertheless, the interactions of the stretch formed from the meeting of the unloading wave in the material and the reflected wave from the solid wall leads to a totally different fragmentation area at t = 13.5 μs. For the chevron and sine wave, the fractured zones behind the metal main body are much larger than those from the other defects, which are less obvious.

For further analyze of the velocity and spatial distributions of the jet particles, Figure 8 and Figure 9 show the velocity distribution and density distribution around the ejecta head on the symmetrical axis at t = 13.5 μs. Figure 8 show that the ejecta head velocities of the chevron and sine wave cases are 6.28 and 5.88 km/s, respectively, and hardly any discrete velocity distribution can be detected in the front of the ejecta in either defect condition. Figure 9 shows that the

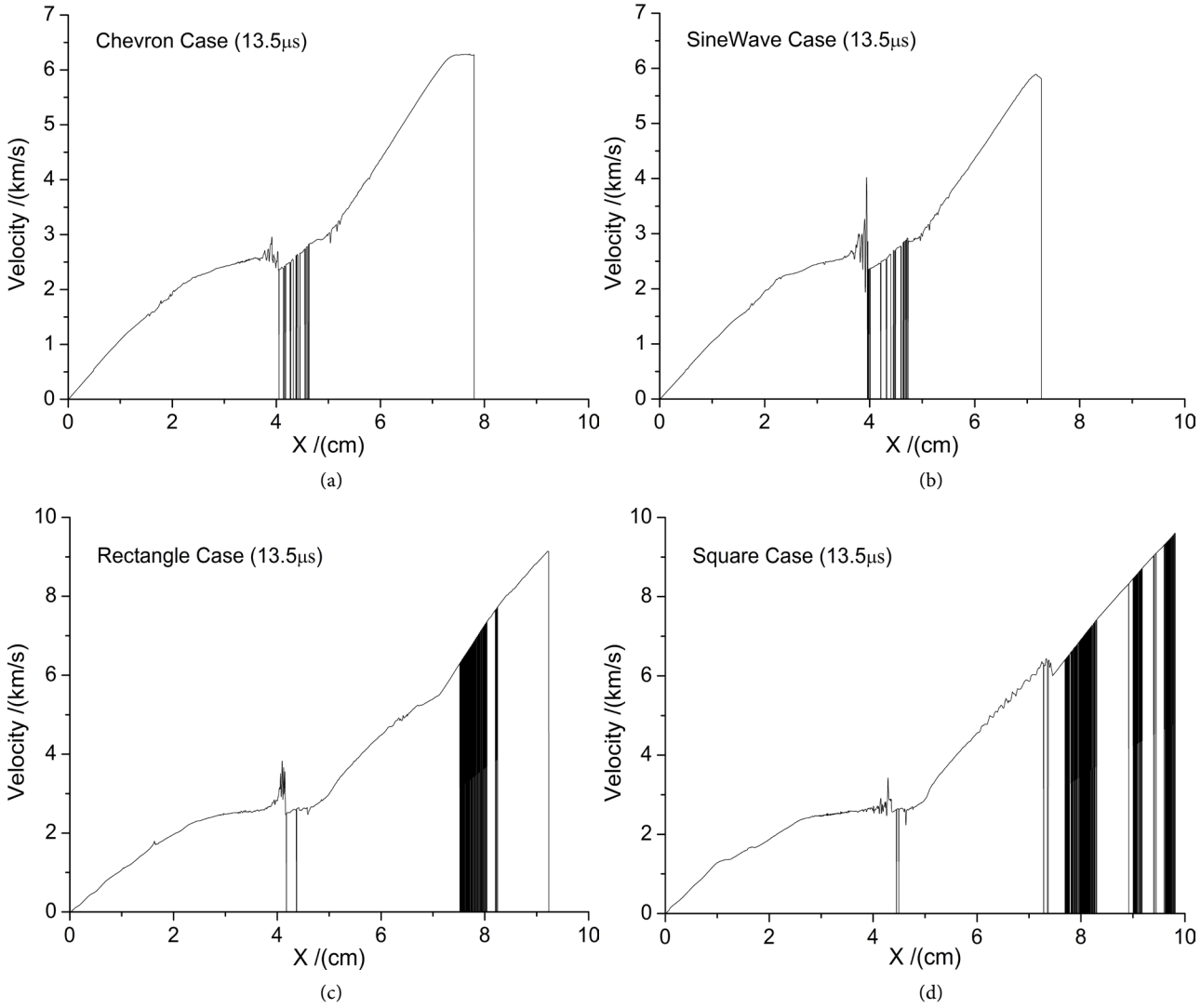

Figure 8. Velocity distributions on the asymmetrical axis for the four defects at $t = 13.5$ μs: (a) chevron; (b) sine wave; (c) rectangle; and (d) square.

low-density area can be found only in part of the ejecta head, indicating that there is tensile stress in the material, without any fragmentation. This explains why no discrete broken particles are found in the front of the ejecta and why only fragmentation can be found in the main body owing to the stretch. However, the ejecta velocities for the rectangle and square are even higher than in the former two conditions, and the highest velocities reach 9.14 and 9.59 km/s, respectively. Additionally, the discrete density distributions are distinctly presented in **Figure 9**, as are the density distributions. The density near the ejecta head is zero, indicating that most of the material fragments are the result of multilayer spallation. Therefore, in the rectangle and square conditions, discrete particles are mainly located in the front area of the ejecta, and the degree of fragmentation is minor in the main body. **Figure 9(c)** and **Figure 9(d)** demonstrate the distribution of the ejecta particles in the rectangle and square conditions. The particles in the rectangle are distributed mainly in the domains of 7.47 - 8.06

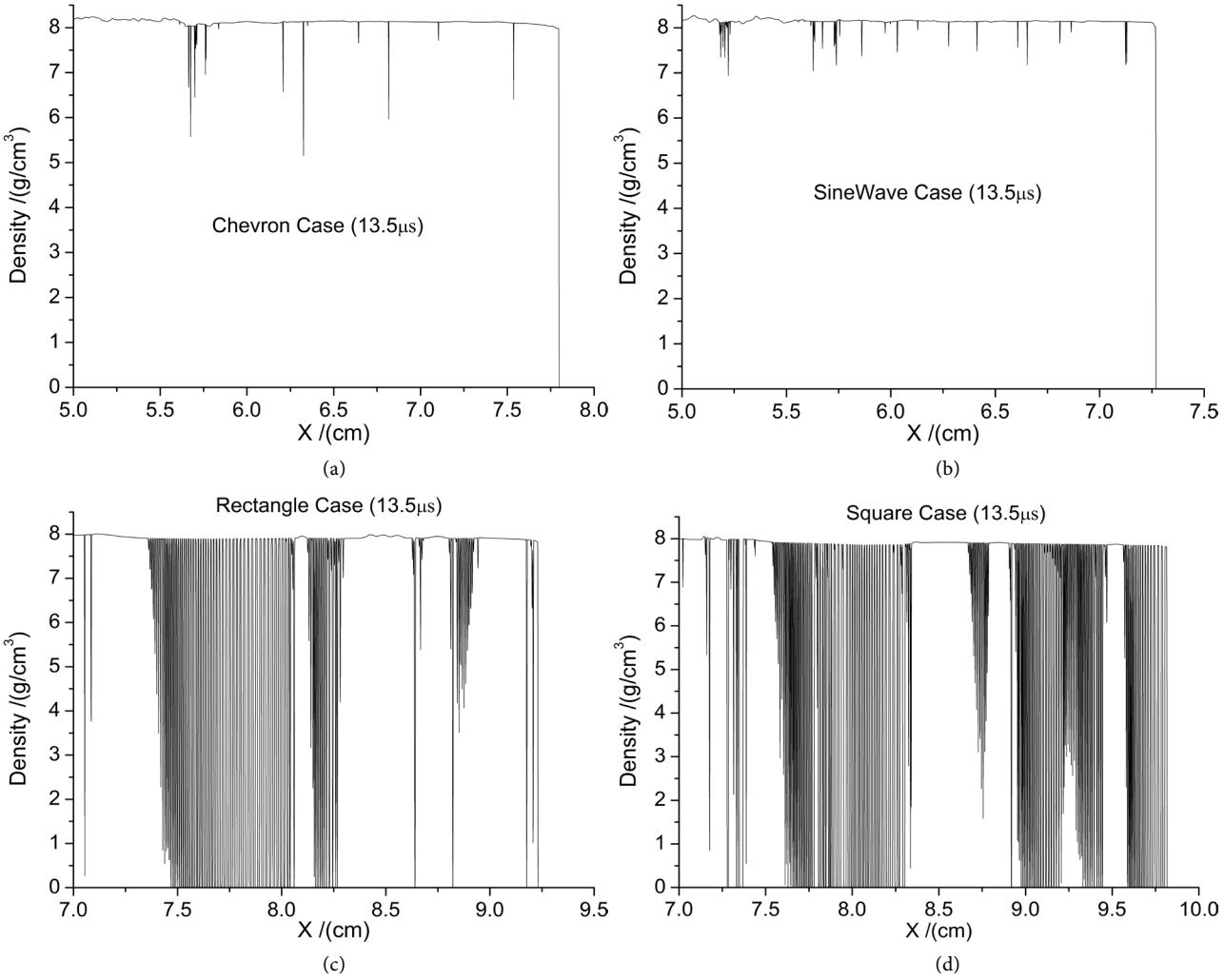

Figure 9. Density distributions around the ejecta head on the asymmetrical axis in the four cases at t = 13.5 μs: (a) chevron; (b) sine wave; (c) rectangle; and (d) square.

and 8.16 - 8.27 cm. For the square, the particle distribution domains are 7.61 - 8.30, 8.92 - 9.19, 9.33 - 9.44, and 9.59 - 9.82 cm, so the conclusion may be drawn that the square undergoes more serious fragmentation than the rectangle. On a macro level, both ejecta heads of the square and rectangle are in a high-speed, low-density area in the particle state. At the same time, the fragmentations and the distribution are closely connected with the initial defect shape. To further understand the particles' thermodynamic state, Figure 10 shows the pressure and temperature distributions of the particles around the ejecta head. From Figure 10 we see that the pressure of the particles under the rectangle and square conditions is almost zero. The particle temperature has reached 1350 - 1700 K, and at some points it even climbs to Cu's melting temperature (~1400 K).

5. Conclusions

By considering four kinds of typical macro defect (chevron, sine wave, rectangle, and square) perturbations on a Cu free surface, our research in the present work

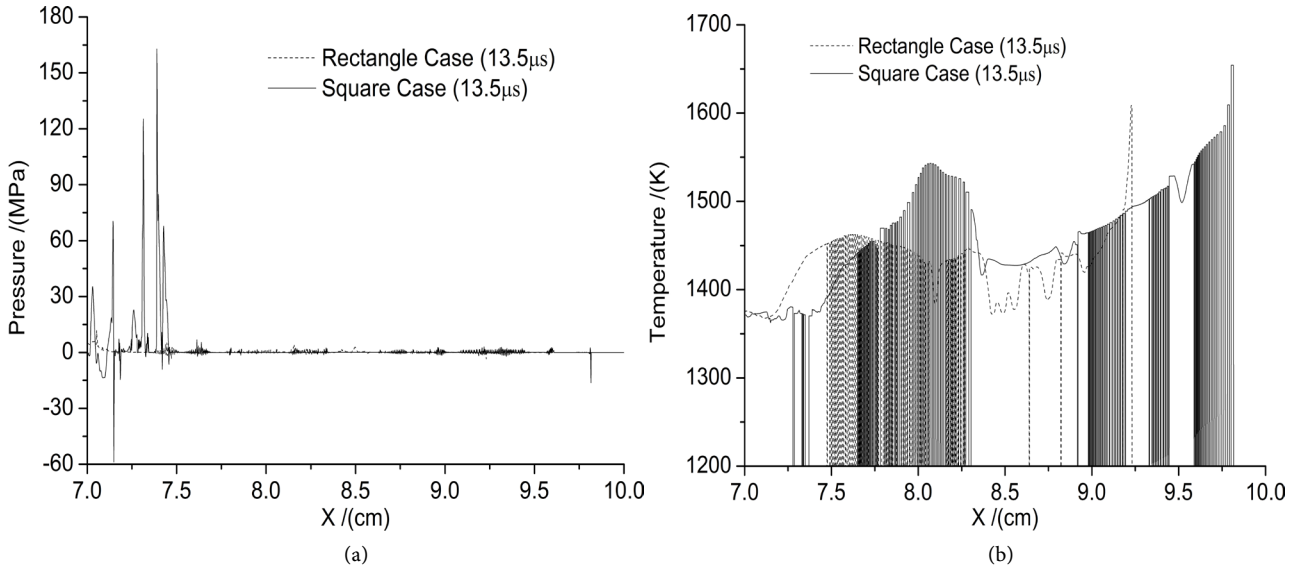

Figure 10. Pressure (a) and temperature (b) distributions around the ejecta head on the asymmetry axis at $t = 13.5$ μs.

mainly focuses on the interface instability, fragmentation, and jetting under a reflected shock wave. Through numerical simulation, we quantitatively compared the different defects and concluded that the interface instability, fragmentation, and ejecta all originate from the initial interface defect and are also associated closely with the shape of the defect. According to the above findings, in the chevron and sine wave cases, the ejecta mass velocities of the head are 6.28 and 5.88 km/s, respectively. Some parts of the inner material are found in a tensile state without any fragmentation, which appears only in the main body of the metal owing to the tension effect. Additionally, for the other two initial perturbations (rectangle and square), the highest ejecta mass velocities are 9.14 and 9.59 km/s, respectively. Fragmentation appears in the large range of shaped pole owing to the multilayer spallation. There is a granule area with high-speed and low-density in the ejecta head. However, the degree of fragmentation is much lower in the main body of Cu. Overall, the jet masses under the four defect conditions vary greatly. Moreover, their time-dependent eject mass follow different law.

Although the Euler method we utilized to calculate the material failure under the stretch strength has met the convergence requirements for conserved quantities, the sizes of the fragmentation area and of the smallest particle are still related to the computational grid size. Our future work will be directed to large-scale computing under a micrometer and to submicron grid size. With the combination of the dynamic experimental data, the best computational size is likely to be obtained. Therefore, our simulation ability will be developed from macro to micro scale. Moreover, because of the complex thermodynamic processes during loading and unloading, establishing a correct constitutive model and EOS will be crucial to improving the reliability of out numerical simulations, and considerably more work remains to be done to study the physical factors that influence the interface instability, fragmentation, and ejecta.

Acknowledgements

The authors would like to thank the supported by "Science Challenge Project" (No. TZ2016001), the National Natural Science Foundation of China (Nos. 11372294 and 11532012), and the Foundation of National Key Laboratory of Shock Wave and Detonation Physics (No. 9140C670301150C67290).

References

[1] Barnes, J.F., Blewett, P.J., McQueen, R.G., Meyer, K.A. and Venable, D. (1974) Taylor Instability in Solids. *Journal of Applied Physics*, **45**, 727-732. https://doi.org/10.1063/1.1663310

[2] Drucker, D.C. (1980) Taylor Instability of the Surface of an Elastic-Plastic Plate. *Mechanics Today*, **5**, 37-47. https://doi.org/10.1016/B978-0-08-024249-1.50013-3

[3] Barnes, J.F., Janney, D.H. and London, R.K., *et al.* (1980) Further Experimentation on Taylor Instability in Solids. *Journal of Applied Physics*, **51**, 4678-4679. https://doi.org/10.1063/1.328339

[4] Lindquist, M.J., Cavallo, R.M., Lorenz, K.T., *et al.* (2006) Aluminum Rayleigh Taylor Strength Measurements and Calculations. Paper Presented at the Tenth International Workshop on the Physics of Compressible Turbulent Mixing, Paris, France.

[5] Weber, S.V., Kalantar, D.H., Colvin, J.D., *et al.* (1999) Nova Experiments Examining Rayleigh-Taylor Instability in Materials with Strength (Report No. UCRL-JC-132739). *7th International Workshop on the Physics of Compressible Turbulent Mixing Russian Federal Nuclear Center-Institute of Experimental Physics*, St. Petersburg, 6 October 1999.

[6] Edwards, J., Lorenz, K.T., Remington, B.A., *et al.* (2004) Laser-Driven Plasma Loader for Shockless Compression and Acceleration of Samples in the Solid State. *Physical Review Letters*, **92**, Article ID: 075002. https://doi.org/10.1103/PhysRevLett.92.075002

[7] Lorenz, K.T., Edwards, M.J., Glendinning, S.G., *et al.* (2005) Accessing Ultrahigh-Pressure, Quasi-Isentropic States of Matter. *Physics of Plasmas*, **12**, Article ID: 056309. https://doi.org/10.1063/1.1873812

[8] Lorenz, K.T., Edwards, M.J., Jankowski, A.F., *et al.* (2006) High Pressure, Quasi Isentropic Compression Experiments on the Omega Laser. *High Energy Density Physics*, **2**, 113-125. https://doi.org/10.1016/j.hedp.2006.08.001

[9] Park, H.-S., Remington, B.A., Becker R.C., *et al.* (2010) Strong Stabilization of the Rayleigh-Taylor Instability by Material Strength at Megabar Pressures. *Physics of Plasmas*, **17**, Article ID: 056314. https://doi.org/10.1063/1.3363170

[10] Smalyuk, V.A., Casey, D.T., Clark, D.S., *et al.* (2014) First Measurements of Hydro-Dynamic Instability Growth in Indirectly Driven Implosions at Ignition-Relevant Conditions on the National Ignition Facility. *Physical Review Letters*, **112**, Article ID: 185003.

[11] Aprelkov, O.N., Ignatova, O.N., Igonin, V.V., *et al.* (2007) Twinning and Dynamic Strength of Copper during High Rate Strain. *AIP Conference Proceedings*, **955**, 619-622.

[12] Atchison, W.L., Zocher, M.A. and Kaul, A.M. (2008) Studies of Material Constitutive Behavior Using Perturbation Growth in Explosive and Magnetically Driven Liner Systems. *Russian Journal of Physical Chemistry B*, **2**, 387-401. https://doi.org/10.1134/S199079310803010X

[13] Igonin, V.V., Ignatova, O.N., Lebedev, A.I., *et al.* (2009) Influence of Dynamic Properties on Perturbation Growth in Tantalum. *AIP Conference Proceedings*, **1195**, 1085-1088. https://doi.org/10.1063/1.3294990

[14] Chen, H.Y., Zeng, J.R., Wang, S.J., *et al.* (1997) Experimental Study of Interface Instability in Cylindrical Convergent Geometry. *Detonation and Shock Waves*, **1**, 1-4.

[15] Lin, Q.W., Xia, X.G. and Zhang, G.R. (1997) Theoretical Calculation of Interface Instability under Cylindrical Convergent Shock Wave. *Detonation and Shock Waves*, **4**, 33-36.

[16] Wang, T., Bai, J.S., Cao, R.Y., *et al.* (2017) Experimental and Numerical Investigations of Perturbation Growth in Aluminium Flyer Driven by Explosion. Manuscript Submitted for Publication.

[17] Meyer, K.A. and Blewett, P.J. (1971) Some Preliminary Numerical Studies of Taylor instability which Include Effects of Material Strength. Report No. LA-4754-MS UC-34.

[18] He, C.J., Zhou, H.B. and Hang, Y.H. (2009) Numerical Analysis of Metal Interface Instability of Aluminum Driven by Detonation. *Science in China Series G*: *Physics, Mechanics & Astronomy*, **39**, 1170-1173.

[19] Bai, J.S., Liu, J.H., Wang, T., *et al.* (2010) Investigation of the Richtmyer-Meshkov Instability with Double Perturbation Interface in Nonuniform Flows. *Physical Review E*, **81**, Article ID: 056302. https://doi.org/10.1103/PhysRevE.81.056302

[20] Bai, J.S., Zou, L.Y., Wang, T., *et al.* (2010) Experimental and Numerical Study of the Shock-Accelerated Elliptic Heavy Gas Cylinders. *Physical Review E*, **82**, Article ID: 056318. https://doi.org/10.1103/PhysRevE.82.056318

[21] Bai, J.S., Wang, B., Wang, T., *et al.* (2012) Numerical Simulation of the Richtmyer-Meshkov Instability in Initially Nonuniform Flows and Mixing with Reshock. *Physical Review E*, **86**, Article ID: 066319. https://doi.org/10.1103/PhysRevE.86.066319

[22] Steinberg, D.J., Cochran, S.G. and Guinan, M.W. (1980) A Constitutive Model for Metals for Applicable at High-Strain Rate. *Journal of Applied Physics*, **51**, 1498-1504. https://doi.org/10.1063/1.327799

[23] Colvin, J.D., Legrand, M., Remington, B.A., Schurtz, G. and Weber, S.V. (2003) A Model for Instability Growth in Accelerated Solid Metals. *Journal of Applied Physicis*, **93**, 5287-5301. https://doi.org/10.1063/1.1565188

Call for Papers

World Journal of Mechanics (WJM)

ISSN 2160-049X (Print) ISSN 2160-0503 (Online)

http://www.scirp.org/journal/wjm

World Journal of Mechanics **(WJM)** is an international peer-reviewed journal dedicated to presenting the English original research studies, reviews in the general field of mechanics including the mechanics of solids, structures and fluids and their interaction.

Subject Coverage

This journal invites original research and review papers that address the following issues. Topics of interest include, but are not limited to:

- Applied Mathematics and Mechanics
- Biomechanics and Modeling in Mechanobiology
- Celestial Mechanics and Dynamical Astronomy
- Classical and Quantum Aspects of Mechanics
- Computational Mechanics
- Computer Methods in Applied Mechanics and Engineering
- Continuum Mechanics and Thermodynamics
- Damage Mechanics
- Dynamics and Vibration Control
- Elasticity and Plasticity
- Engineering Fracture Mechanics
- Environmental Fluid Mechanics
- Experimental Mechanics
- Fluid Mechanics and Aerodynamics
- Mathematical Fluid Mechanics
- Mathematics and Mechanics of Solids
- Mechanical Behavior of Biomedical Materials
- Mechanical Engineering Science
- Mechanical Systems and Signal Processing
- Mechanics & Astronomy
- Mechanics and Materials in Design
- Mechanics in Medicine and Biology
- Mechanics of Materials
- Mechanics of Time-Dependent Materials
- Microfluidics
- Micromechanics and Microengineering
- Multi-Scale Mechanics
- Nanomechanics
- Non-Linear Mechanics
- Non-Newtonian Fluid Mechanics
- Numerical and Analytical Methods in Geomechanics
- Probabilistic Engineering Mechanics
- Rock Mechanics and Mining Sciences
- Solid and Structural Mechanics
- Statistical Mechanics and Its Applications
- Terramechanics
- Theoretical and Applied Fracture Mechanics
- Thermophysics and Aeromechanics
- Thin Film Mechanics
- Viscoelasticity

We are also interested in short papers (letters) that clearly address a specific problem, and short survey or position papers that sketch the results or problems on a specific topic. Authors of selected short papers would be invited to write a regular paper on the same topic for future issues of World Journal of Mechanics.

Notes for Intending Authors

Submitted papers should not have been previously published nor be currently under consideration for publication elsewhere. Paper submission will be handled electronically through the website. All papers are refereed through a peer review process. For more details about the submissions, please access the website.

Website and E-Mail

http://www.scirp.org/journal/wjm **E-mail: wjm@scirp.org**

What is SCIRP?

Scientific Research Publishing (SCIRP) is one of the largest Open Access journal publishers. It is currently publishing more than 200 open access, online, peer-reviewed journals covering a wide range of academic disciplines. SCIRP serves the worldwide academic communities and contributes to the progress and application of science with its publication.

What is Open Access?

All original research papers published by SCIRP are made freely and permanently accessible online immediately upon publication. To be able to provide open access journals, SCIRP defrays operation costs from authors and subscription charges only for its printed version. Open access publishing allows an immediate, worldwide, barrier-free, open access to the full text of research papers, which is in the best interests of the scientific community.

- High visibility for maximum global exposure with open access publishing model
- Rigorous peer review of research papers
- Prompt faster publication with less cost
- Guaranteed targeted, multidisciplinary audience

Scientific Research Publishing

Website: http://www.scirp.org

Subscription: sub@scirp.org

Advertisement: service@scirp.org